EXPERIMENTAL STUDY ON THE PERFORMANCE OF COARSE GRAIN MATERIALS AS SCOUR PROTECTION

Alexander Schendel[1], Nils Goseberg[1,2] and Torsten Schlurmann[1]

Large scale hydraulic model tests were carried out to investigate the erosive potentials, bed stability and the performance as scour protection of wide-graded quarry-stone material with fractions ranging from 0.063 – 200 mm. Within the two phase test program the material was exposed to several wave spectra during hydraulic model tests in the Large Wave Flume of the Forschungszentrum Küste and additionally to an incrementally increased current in a closed-circuit flume at the Franzius-Institute. As result of the wave load, a maximum scour depth of S/D = 0.161 was observed after 9000 waves with a simulated storm duration of 20 h in model scale. Furthermore, fractional critical shear stresses were determined based on velocity measurements, which indicate highly selective incipient motion of individual fractions under steady current conditions. The selective mobility of this wide-graded material could not be expressed by the Shields approach.

Keywords: scour protection, hydraulic model test, wide-graded grain material, erosion stability, incipient motion, critical shear stress

Introduction and Motivation

As a result of the progressing expansion and accelerated development of Offshore Wind Energy Converters the need for economically and technically optimized scour protection systems increases likewise to guarantee long term operation of supporting structures in various locations. Due to their versatility and cost efficiency wide-graded material mixtures, mainly composed of artificial quarry-stone material, are considered a potential scour protection system, which can meet the requirements of structures in fluvial, estuarine and coastal waters. The main reason for this is that wide-graded materials can be applied as single layer scour protection, which simplifies the way of installing the protective layer by excavators or slides. In such application, the verification of the stability of wide-graded material mixtures with respect to external forces exerted by currents or waves is of major importance.

However, up to date fundamental research studies, which can verify the stability of wide-graded material mixtures under offshore conditions as well as their actual performance as scour protection system are scarce. The applicability of existing approaches and guidelines for the design of scour protection for offshore supporting structure has not yet been validated for the material under consideration. Furthermore, the numerous studies on the erosion stability of wide-graded material mixtures are mostly based on fluvial erosion and sedimentation processes and thereof linked to material properties and flow conditions, which are dominant in hydraulic engineering. On this account, the results of those studies cannot be directly transferred to the stability of wide-graded quarry-stone materials under offshore conditions. In light of this situation, industry-funded large-scale hydraulic model tests were conducted by the Franzius-Institute for Hydraulic, Estuarine and Coastal Engineering at Leibniz University Hannover, Germany, in order to investigate fundamentals of erosive potentials, bed stability and the performance as scour protection of wide-graded material mixtures. On this basis safer and more economic design criteria for scour and bed protection are sought. A two phase experimental test program firstly contained the assessment of the performance as adaptable and "low-regret" scour protection for maritime structures und typical wave loads by carrying out hydraulic model tests in the Large Wave Flume (GWK) of the Forschungszentrum Küste (FZK) in Hannover. Based on the findings in the first phase, a second phase was conducted with the purpose to describe the characteristic erosion and sedimentation processes as well as to quantitatively determine the bed stability of a wide-graded grain material under steady flow conditions. The model tests of the second phase were carried out in the closed-circuit flume of the Franzius-Institute.

In accordance with the two phase test program this paper is equally organized in two parts. A first part describes the experimental setup and presents the results of the model tests in the Large Wave Flume while the second part focuses on the steady current experiments in the closed-circuit flume. At the end combined conclusions for both parts will be drawn.

[1] Franzius-Institute for Hydraulics, Estuarine and Coastal Engineering, Leibniz University Hannover, Nienburger Str. 4, 30167 Hannover, Germany
[2] Department of Civil Engineering, University of Ottawa, 161, Louis Pasteur St., Ottawa, Ontario, K1N 6N5, Canada

SCOUR PERFORMANCE UNDER SPECTRAL WAVE LOADS

Experimental setup

The hydraulic model tests were carried out in the Large Wave Flume of the Forschungszentrum Küste at a model scale of 1:4. This model scale was particularly chosen to account for scaling and model effects with regard to the unique sediment properties. The investigated material was a wide-graded quarry-stone material made of Jelsa-Granodiorite with a grain size distribution of 0.063-200 mm. Due to the abundance of finer fractions within the grain size distribution and the sharp-edged grain shapes, the tested material significantly differed from material mixtures used in previous studies. Fig. 1 shows the grain size distribution of the original material and also depicts the slightly deviating distribution of the scaled material in 1:4 model scale. Tab. 1 additionally presents some key properties of the investigated material.

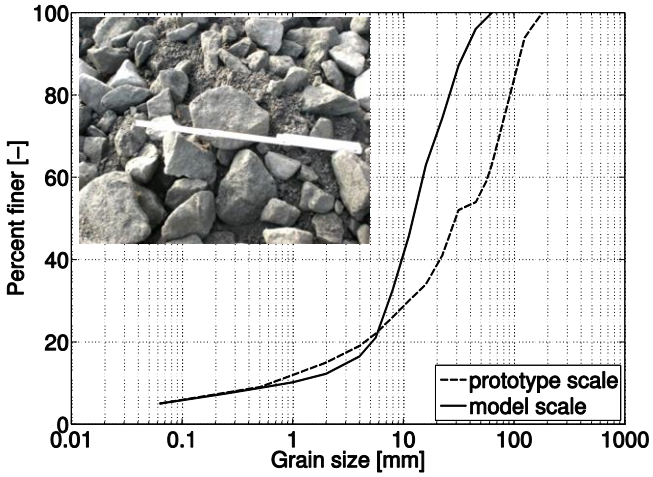

Figure 1: Original and scaled grain size distribution of tested wide-graded grain material (semi-logarithmic). Inset depicts an image of one actual material surface in a big pack right after the transport together with a metric folding rule.

Table 1: Grain size and gradation characteristics of material in prototype and model scale.

Material	d_{10} [mm]	d_{16} [mm]	d_{30} [mm]	d_{50} [mm]	d_{60} [mm]	d_{84} [mm]	Cu [-]	Cc [-]
Prototype scale	0.6	2.5	11.2	30	62	102	103	3.37
Model scale	1.0	4.0	7.4	12.0	15.0	29.5	15	3.65

The Large Wave Flume is 307 m long, 7 m deep and 5 m wide. The waves are generated by a piston type wave generator with maximum stroke of ± 2.1 m. Regular waves up to a height of 2.00 m and wave spectra with a maximum significant wave height of H_s = 1.3 m can be generated under model conditions. Furthermore, the wave machine is able to filter re-reflections by an active custom-made absorption system. The model setup consisted of two independent test sections. While the first section provided the assessment of the general bed stability of the wide-graded material under spectral wave load, the second section (Figs. 2 and 3) followed the investigation of the structure-induced scour and protection around a monopile-support structure. This present paper only refers to the results of the second section for brevity. The setup for the second section included a monopile as offshore foundation structure with a diameter of D = 1 m. The monopile was placed in the middle of a single layer material bed made of the wide-graded material mixture. The material bed was installed with a layer thickness of 0.5 m over a length of 9 m and ended on both sides of the wave flume. It has to be noted that with this setup the negative effects of secondary scours and material sinking into the underlying sediment were prevented.

For the continuous measurement of water surface elevation a total number of 20 wire-type wave gauges were installed along the flume side. Besides, 6 ADV probes were used for the determination of the orbital velocity distribution under waves. The measurement of the scour process and the general

material displacement around the monopile was conducted by the combination of Acoustic Backscatter Systems (ABS, AQUAscat 1000L), single-beam Echosounders (Tritech PA 500/6- PS) and the first-time application of a high resolution 3D laser scanner (FARO Focus^{3D}). The high resolution scans (accuracy up to ± 2 mm, depending on the distance to the object) by the laser scanner enabled the determination of smallest displacement processes on the bed, which is a very useful feature when dealing with coarse grain materials. In addition, the bed movement during the tests could be observed with 5 underwater cameras installed in the monopile. The experimental setup as well the placement of the measurement devices are shown in Fig. 2.

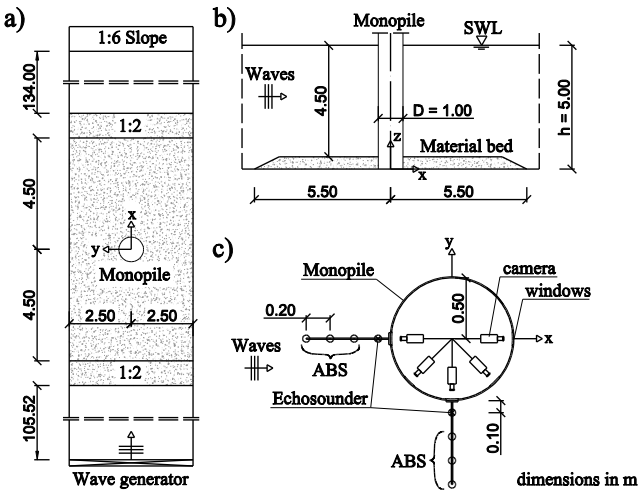

Figure 2: Sketch of the experimental setup: a) Top View; b) Side View; c) Placement of measurement devices around the monopile.

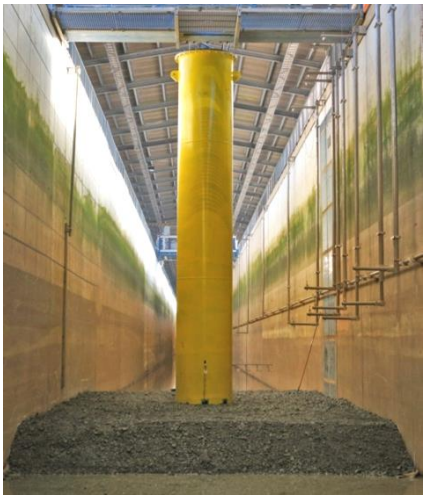

Figure 3: Picture of experimental setup. Waves are propagating in viewing direction.

In order to meet North Sea environmental conditions approximately, the model tests were carried out with spectral wave load (JONSWAP-spectra with $\gamma = 3.3$). The significant wave height H_s was successively increased in three steps from 0.7 m to 1.3 m with a constant peak period $T_p = 8$ s. For each spectrum a total amount of 3000 waves was generated. The water depth remained constant throughout the entire test program at 5 m above the flume bed. The ABS and Echosounder devices allowed a continuous measurement of the scour development, but only at fixed positions close to the monopile. In contrary, the laser scanner which was able to capture the entire scene at once could only be applied after the water had drained. Therefore, only 3 laser scans could be made for each wave spectrum. Tab. 2 gives an overview over the test conditions.

Table 2: Test conditions for scour tests under spectral (JONSWAP) wave loads in model scale. U_m is calculated by linear wave theory with $H = H_s$ and $T = T_p$.

Spectrum	Number of waves	Wave length	Significant wave height	Peak wave period	Maximum horizontal orbital velocity	Keulegan-Carpenter number
	N	L	H_s	T_p	U_m	KC
	[-]	[m]	[m]	[s]	[m/s]	[-]
01	3000	53.1	0.7	8.0	0.51	4.1
02	3000	53.1	1.0	8.0	0.73	5.9
03	3000	53.1	1.3	8.0	0.96	7.6

Qualitative material performance under wave load

In this chapter qualitative impressions of the general material behavior under wave load is presented based on observations by eye during the model test. While the scour development induced by the first wave spectrum was relatively small and a distinct position of a maximum scour could not be

determined visually, the scour development increased significantly during the second and third wave spectrum based on increasing significant wave height H_s.
Despite the further development of the scour depth during the third spectrum an overall high stability under wave loads can be attributed to the material. To demonstrate this observation the small scour development at the end of the test is shown in Fig. 4. Moreover, tendencies of a developing armor layer on the bed surface became visible after the first wave spectrum with H_s = 0.7 m (red circle in Fig. 5). This is consistent with results from the additional model tests applying steady flow conditions as reported in the next chapter of this paper. In addition, a beginning sorting of material fractions especially around the monopile was found as illustrated in Fig. 5. A deposition of finer material fractions occurred directly at the sides of the monopile (blue circle). In contrast, coarser material fractions concentrated in a wider radius around the monopile (yellow circle in Fig. 5). The development of the deposition of finer fractions at the sides of the monopile could also be directly observed by the cameras mounted inside the monopile (Fig. 6).

Figure 4: Final scour development around the monopile after 9000 waves and maximum significant wave height H_s = 1.3 m. Waves are propagating in the direction of view.

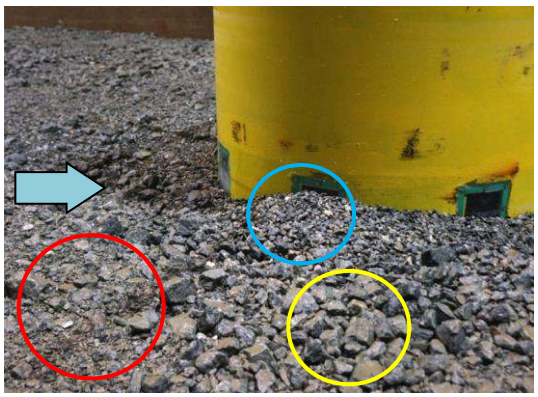

Figure 5: Tendencies of armor layer development (red circle), deposition of finer fractions on the sides (blue circle) and coarser fractions (yellow circle) around the monopile after 3000 waves with H_s = 0.7 m. Waves are coming from the left side.

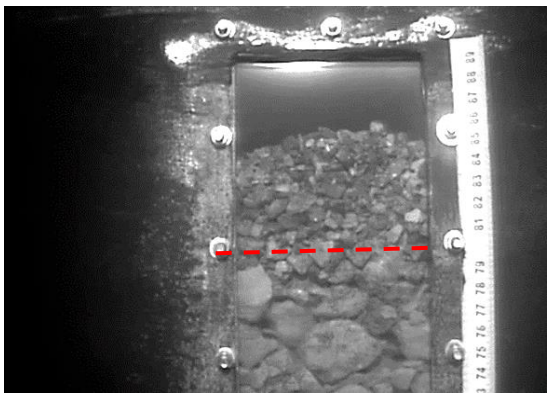

Figure 6: Deposition of finer fractions at the sides of the monopile after 3000 waves with H_s = 0.7 m. Red line indicates initial bed level.

Structure-induced scour development under irregular waves

The following Figs. 7-9 showcase the scour development around the monopile based on the laser scan analysis. In these figures scour is represented in blue color, while depositional development is plotted in red. In order to account for potential measurement uncertainties only changes in bed topography greater than ± 5 mm were considered. Within the first spectrum (H_s = 0.7 m) a symmetrical scour developed around the monopile with maximum scour depths in front and depositions at both sides of the structure (Fig. 7). As a result of the second spectrum (H_s = 1.0 m) the maximum scour depth diagonal in front of the monopile increased. In addition, a second concise scour was formed on

the back side of the monopile. Furthermore, the increased load leads to an asymmetrical scour pattern in wave direction. The inhomogeneous material composition as well as an inevitable uneven compaction during the installation of the material in the flume may be possible explanations for the asymmetrical scour pattern. Apart from that, a typical radial scour developed as the third wave spectrum with H_s = 1.3 m was exposed to the monopile. Afterwards, two positions with almost identical maximum scour depth were identified. The first (position 1 in Fig. 10) is located diagonal in front of the monopile at x/D = 0.67 and y/D = 0.72 in relation to the center of the monopile. The second (position 2 in Fig. 10) is placed behind the monopile at x/D = 1.29 and y/D = 0.13.

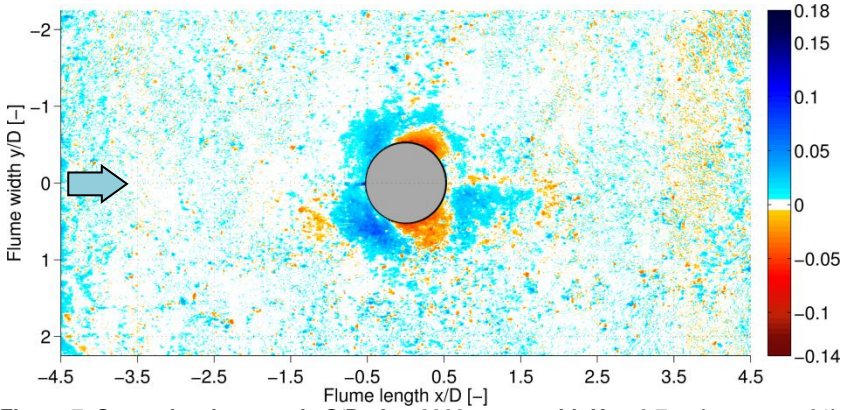

Figure 7: Scour development in S/D after 3000 waves with H_s = 0.7 m (spectrum 01).

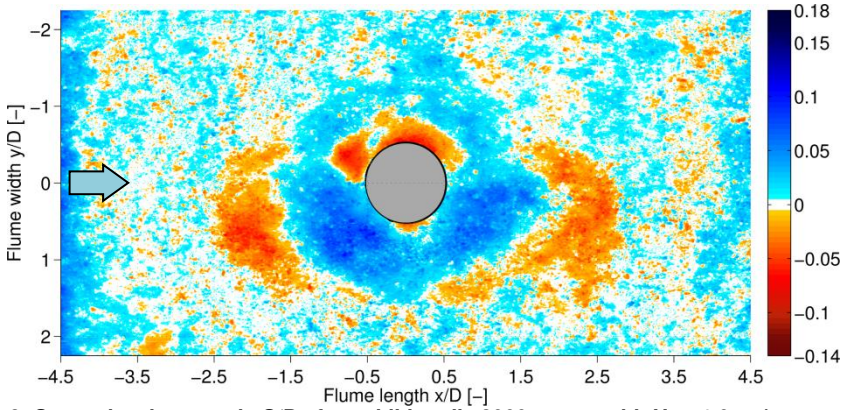

Figure 8: Scour development in S/D after additionally 3000 waves with H_s = 1.0 m (spectrum 02).

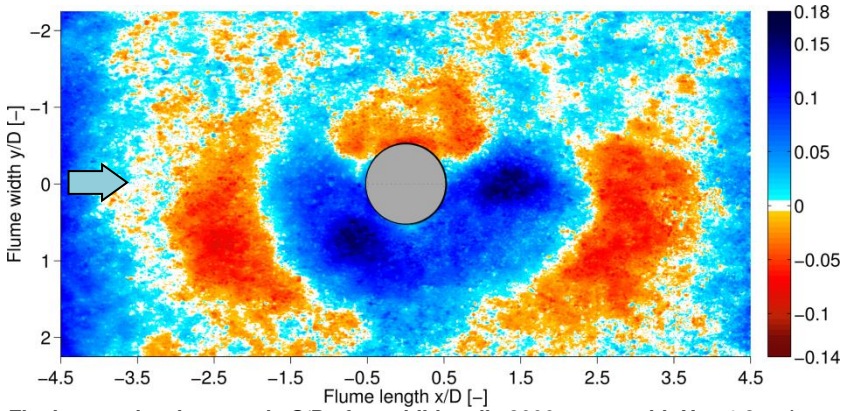

Figure 9: Final scour development in S/D after additionally 3000 waves with H_s = 1.3 m (spectrum 03).

Due to the successive wave load with increasing H_s, the combined development of the maximum scour depth for all three spectra is given in Fig. 10. In the beginning of each spectra, and thus with every step up of H_s, the maximum scour depth increased considerably. In the further course of a spectrum the increase of scour depth slowed down. In summary, a maximum scour depth of S/D = 0.161 was observed after 9000 waves and a applied storm duration of 20 h with a maximum significant wave height of H_s = 1.3 m. This maximum scour depth found in the experimental investigation is

significantly below practical design approaches for scour depth estimation at monopiles with S/D = 1.3 (DNV, 2010) or S/D = 2.5 (GL, 2005). However, it should be noted that a wave load of 3000 waves for each wave spectrum has proven to be insufficient to achieve an equilibrium scour depth, so that a further increase of scour depth with ongoing wave load has to be assumed. The detailed development of scour depth for each wave spectrum can be taken from Tab. 3. Since the ABSs and Echosounders were not able to measure the maximum scour depth the displayed development of the maximum scour depth is based and the laser scanner data only.

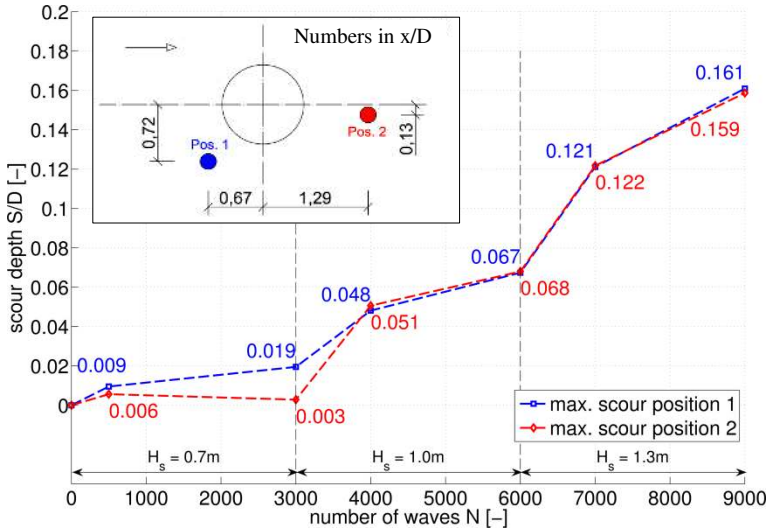

Figure 10: Development of maximum scour depth for position 1 (blue) and position 2 (red), combined for all wave spectra.

Table 3: Maximum scour depth and accumulated maximum scour depth for position 1 and position 2 for every measurement based on laser scanner data.

Spectrum	Number of waves	Position 1 Maximum scour depth	Position 1 cumulative maximum scour depth	Position 2 Maximum scour depth	Position 2 cumulative maximum scour depth
	N	S/D_{max}	$\Sigma\ S/D_{max}$	S/D_{max}	$\Sigma\ S/D_{max}$
	[-]	[-]	[-]	[-]	[-]
1	500	0.009		0.006	
	2500	0.010	0.019	-0.003	0.003
2	1000	0.029		0.048	
	2000	0.019	0.048	0.017	0.065
3	1000	0.054		0.054	
	2000	0.040	0.094	0.037	0.091
Σ	9000		0.161		0.159

By cumulating the scour processes over the considered bed surface around the monopile the displaced scour volume is calculated. Fig. 11 shows the cumulated scour volume in dependency to the radial distance r/D to the monopile center. In regard to the development of the maximum scour depth, the amount of eroded scour volume increased at the beginning of each wave spectrum. Here, the highest displaced scour volume per m² surface area could be determined within a distance of r/D = 1.5 to the center of the monopile. Beyond this distance the scour volume decreased, due to the deposition of material at a distance of r/D = 2 (Fig. 8 and 9). Further, the development of the scour volume at a distance of r/D = 0.75 (red curve in Figure 11) indicates the described deposition of finer material fractions directly at the sides at the monopile. The maximum scour volume after 9000 waves is

0.05 m³/m², so that an average scour depth of 5 cm (model scale) within a radius of r/D = 1.5 can be found as a result of the successively increasing wave load with a significant wave height H_s up to 1.3 m. At this point, the asymmetric scour pattern has to be pointed out again, which influences the calculation of the radial scour volume around the monopile.

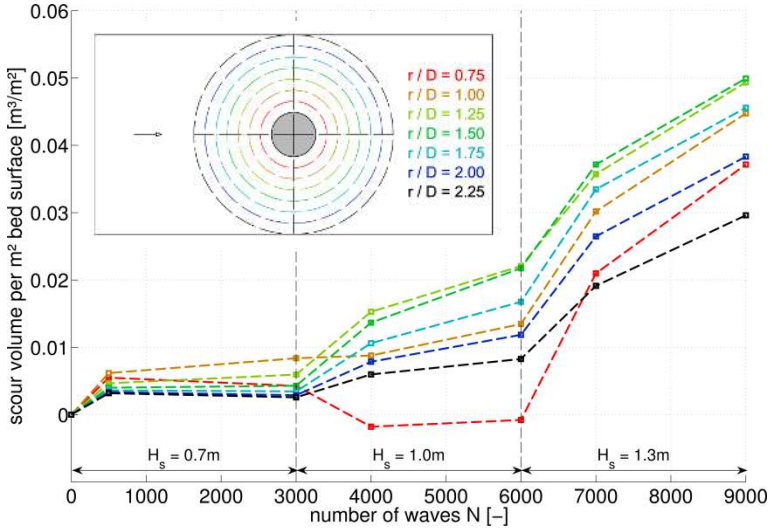

Figure 11: Development of cumulated scour volume around the monopile with increasing number of waves and depending on the radial distance to the monopile center. The scour volume is normalized by the radial surface areas specified in the inset (in model scale).

Discussion

Comparison of this results with practical design guidelines for the scour depth estimation of monopile foundation (GL, 2005; CERC, 2006; DNV, 2010) revealed much smaller scour depth for the innovative scour protection material composed of Jelsa-Granodiorite. However, these guidelines take also into account the combined influence of currents and waves while for the derivation of the published guidelines equilibrium scour depths were obtained. In this present study the number and intensity of the waves exerted to the structure have been too small to achieve an equilibrium scour depth. These results we have presented herein are thus preliminary and it is anticipated that further experiments have to clarify equilibrium scour depth finally.

A direct comparison of this results with approved approaches from the literature on maximum scour depth (Sumer et al., 1992; Melville and Coleman, 2000; Zanke et al., 2011) or time scale of scour development (Sumer and Fredsoe, 2002) cannot be carried out to date due to highly divergent material properties and the successive wave load. Additionally, the hydraulic model tests were conducted in the Large Wave Flume with a relatively large model scale, so that different scaling and model effects have to be considered compared to small scale model tests that were particularly used for the mentioned literature. Also, those approaches are not valid and applicable for small KC number (KC<6) and thus comparability is limited so far. This also underpins the necessity for ongoing testing of the considered material.

EROSION STABILITY UNDER STATIONARY CURRENT

Experimental setup

The hydraulic model tests of the second phase were carried out in the closed-circuit flume of the Franzius-Institute for Hydraulic, Estuarine and Coastal Engineering, University Hannover, Germany. The flume is driven by four pipe pumps with a maximum discharge of 0.5 m³/s. Total length of the flume is 60.0 m with a 3.13 m long window section at the study area were the sediment layer was placed in a pit (Fig. 12). The cross-sectional size of the flume is 1.0 m x 1.0 m with a horizontal and not inclined bottom. Both bottom and flume walls have a floating screed finish. In order to investigate the ongoing erosion processes a prototype model scale of 1:1 was chosen for the model tests. Thereby, scaling effects that could bias the behavior of finer fraction within the wide-graded material could be reduced to a minimum. The wide-graded material was installed in a pit with a width of 1.0 m, a length of 2.7 m and with a layer thickness of 200 mm. The material was placed on top of a sublayer with similar grain characteristics to simulate a natural interlocking with the subsurface. Fig. 12 illustrates the

experimental setup, Fig. 13 shows the material placement in the pit before the flume was filled with water.

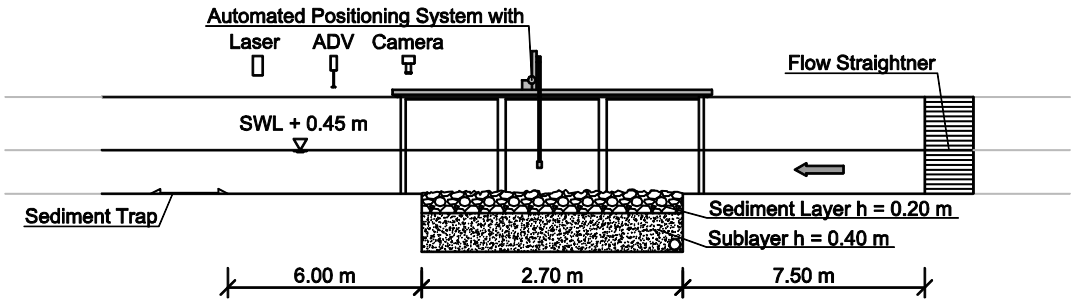

Figure 12: Schematic cross-section of experimental setup (not to scale).

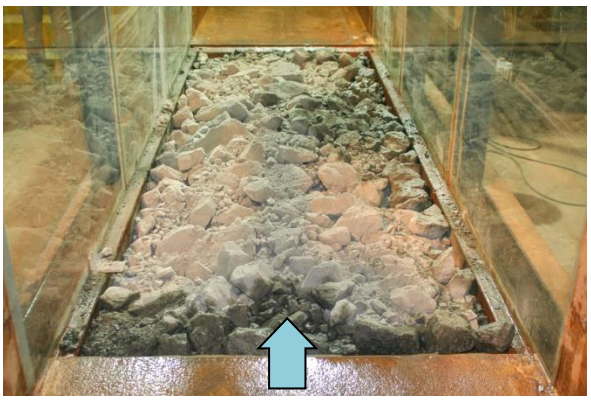

Figure 13: Sediment pit with build-in wide-graded material before water was filled in the flume.

The applied wide-graded material was identical to the prototype material of the first test phase (see Fig. 1 for grain size distribution). For the second test phase three test samples of this material were obtained with slightly different grain size distributions, which resulted in three consecutive experimental runs. Tab. 4 summarizes the grain parameters of the three used material samples.

Changes of the bed topography over time were measured with a laser distance sensor (Baumer OADR 2016480, resolution 0.015 – 0.67 mm) which was mounted on an automated positioning system above the test area. By means of the laser sensor digital elevation models (DEM) of the bed topography were created with a vertical accuracy of about 1.0 mm.

In order to measure the eroded bed load a sediment trap was installed downstream of the sediment bed. The amount as well as the gain size distribution of the eroded bed load were determined for each test run and compared to the grain characteristics of the initial material. Due to its design as an artificial pit trap, the sediment trap was not able to collect suspended material.

By using an acoustic Doppler velocimeter (ADV, NORTEK Vetrino+) 3D velocity measurements were carried out. The positions and heights of the measurements over the sediment bed had to be varied for the three experiments in order to account for the rough bed surface. For each position the measuring period amounted to 30 s with a sampling rate of 200 Hz. The velocity measurements provided the basis for the estimation of bed shear stresses. In combination with the sediment trap results is was possible to assess the bed stability by defining critical shear stresses for individual sediment fractions. Tab. 4 summarizes the test conditions and the grain size distributions with $\bar{u}$ as the mean flow velocity averaged over a cross-sectional area during preliminary test without a sediment bed.

Table 4: Test conditions for all 3 experiments and the grain size distributions of the material samples used in these experiments. The lower section of this table shows the load cases for each experiment.

Experiment	Grain size parameters								Test conditions		
	d_{10} [mm]	d_{16} [mm]	d_{30} [mm]	d_{50} [mm]	d_{60} [mm]	d_{84} [mm]	Cu [-]	Cc [-]	$\bar{u}$ [m/s]	T [min]	H [cm]
A	0.6	2.5	11.2	30	62	102	103	3.37	0.10-0.90	120	45
B	0.4	1.0	5.6	25	56	100	140	1.40	0.10-0.90	120	45
C	1.0	4.0	22.4	72	85	116	85	5.90	0.10-0.90	120	45

Load cases	1	2	3	4	5	6	7
$\bar{u}$ [m/s]	0.10	0.18	0.24	0.38	0.56	0.72	0.90

Experimental procedure

A total amount of three experiments were carried out with repeating load conditions but slightly different material properties (compare Tab. 4). In each experiment the flow velocity was successively increased in seven load cases from 0.1 m/s to 0.9 m/s. Adding up the 2 hours load duration for each flow velocity a cumulated load time of 14 hours for each experiment and material sample was achieved. At the beginning of every load case the flume was carefully filled with water on both sides of the sediment bed. During the experiments no additional sediment was added.

Velocity profiles were measured at 10 positions above the sediment bed, of which 5 positions were located on the longitudinal axis of the flume. The positioning of the remaining profiles was based on distinctive structures within the bed surface, in particular hiding and exposure areas. For each profile the velocity was measured at 8 points over half of the water depth, with an interval of 1 cm between the bed nearest five points and an interval of 5 cm between the remaining three points.

After the experiment was stopped the water was slowly drained in order to enable the scanning of the bed surface with the laser sensor and to remove the collected material out of the sediment trap. Along with the ADV probe the laser sensor was mounted on the automated positioning system. Thereby the bed surface could be scanned in a grid like pattern with a longitudinal spacing of $\Delta x =$ 0.5 mm and a lateral spacing of $\Delta y =$ 5 mm, respectively. To consider wall influences and roughness changes the scan area was reduced by 38 cm on both ends and 10 cm on both sides in relation to the sediment surface, resulting in a total scan area of 80 cm x 194 cm. In this way the sediment topography was scanned after each load case.

Due to the small amount of eroded material in the first 3 load cases, grain size distributions of the eroded material could only be produced for the last 4 load cases.

Applied analysis methodology

Based on the laser scans detailed DEMs of the sediment bed topography were generated. The process included the elimination of spikes in the laser signal and the interpolation of data points to a 1 mm x 1 mm fine grid by means of a cubic Delaunay triangulation. Subsequently, erosion and accumulation areas within the bed surface due to increasing flow velocities could be determined by calculating the elevation difference between DEMs of single load cases.

The present bed shear stresses were estimated on the assumption of a logarithmic velocity distribution within the boundary layer as being applied in Biron at el. (2004) and Petri et al. (2010). Though this log law method involves some uncertainties, especially in such complex and turbulent flow conditions, it also has some advantages. By measuring velocity profiles and fitting a logarithmic equation in form of $\ln z$ to them, the local roughness lengths z_0 for each measurement position can be determined instead of assuming a global roughness length for all measurement positions. In this study the fitting was carried out by using a least square error approach. Furthermore, the goodness of the fitting was measured by the coefficient of determination R^2, at which values of R^2 of over 91 % for all measured profiles could be achieved. Fig. 14 shows the distribution of calculated bed shear stresses for all three experiments and underlines the variation of bed shear stress caused by the extremely rough sediment surface.

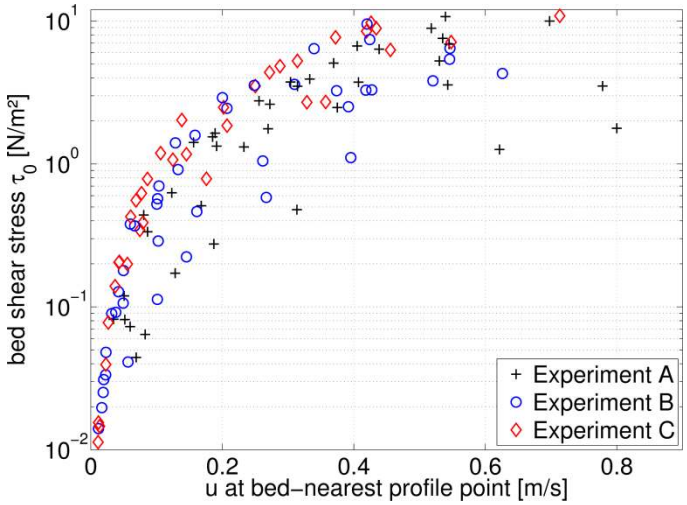

Figure 14: Calculated bed shear stresses in comparison to the measured near bed flow velocities.

For the assessment of the erosion stability under stationary flow the incipient motion condition has to be defined. In this study the calculated bed shear stresses are compared with the largest grain fraction collected by the sediment trap in each load case to determine fractional critical shear stresses $\tau_{c,i}$ and therefore conclude critical conditions for the incipient motion. In accordance with the Largest-Grain Method (described by Wilcock (1988) and applied by Andrews (1983) and Carling (1983)) coarser fractions were still available in the bed in each experiment and load case. In the following, the experimental results, which were obtained on the basis of the above outlined methodology, are presented and discussed.

Changes in bed topography and displacement processes

During the experiments a significant coarsening of the sediment surface with increasing flow velocities due to the selective erosion of finer grain fractions has been visually observed. The increase of the flow velocity led to further erosion of finer material again and again at the beginning of each load case. By the end of each load case a stabile bed surface was provided and sediment transport could no longer be detected, so that the development of a static armor layer can be concluded (Jain, 1990; Marion and Fraccarollo, 1997; Parker and Sutherland, 1990). Furthermore, numerous areas within the bed surface could be identified where stability-affecting exposition and hiding phenomena appeared. The resulting erosion and accumulation areas can be illustrated by creating plots of bed elevation differences between individual load cases based on the DEMs. Fig. 15 exemplarily shows the DEM of the bed topography and the cumulated displacement processes during experiment B.

Along with progressing flow velocities an increase of erosion (blue) and accumulation (red) areas can be found. Thereby, the erosion outweighs the accumulation a few times. At the same time, erosion is taking place globally distributed, and thereby reflecting areas with large quantities of finer fractions, whereas accumulation is locally concentrated behind larger stones or similarly protected parts. While the characteristics of the development of erosion and accumulation areas with increasing flow velocities is similar, considerably difference in the quantity of erosion between all three experiments were detected depending on the varieties in initial grain size distribution, placement and bed surface structure (not shown here for brevity).

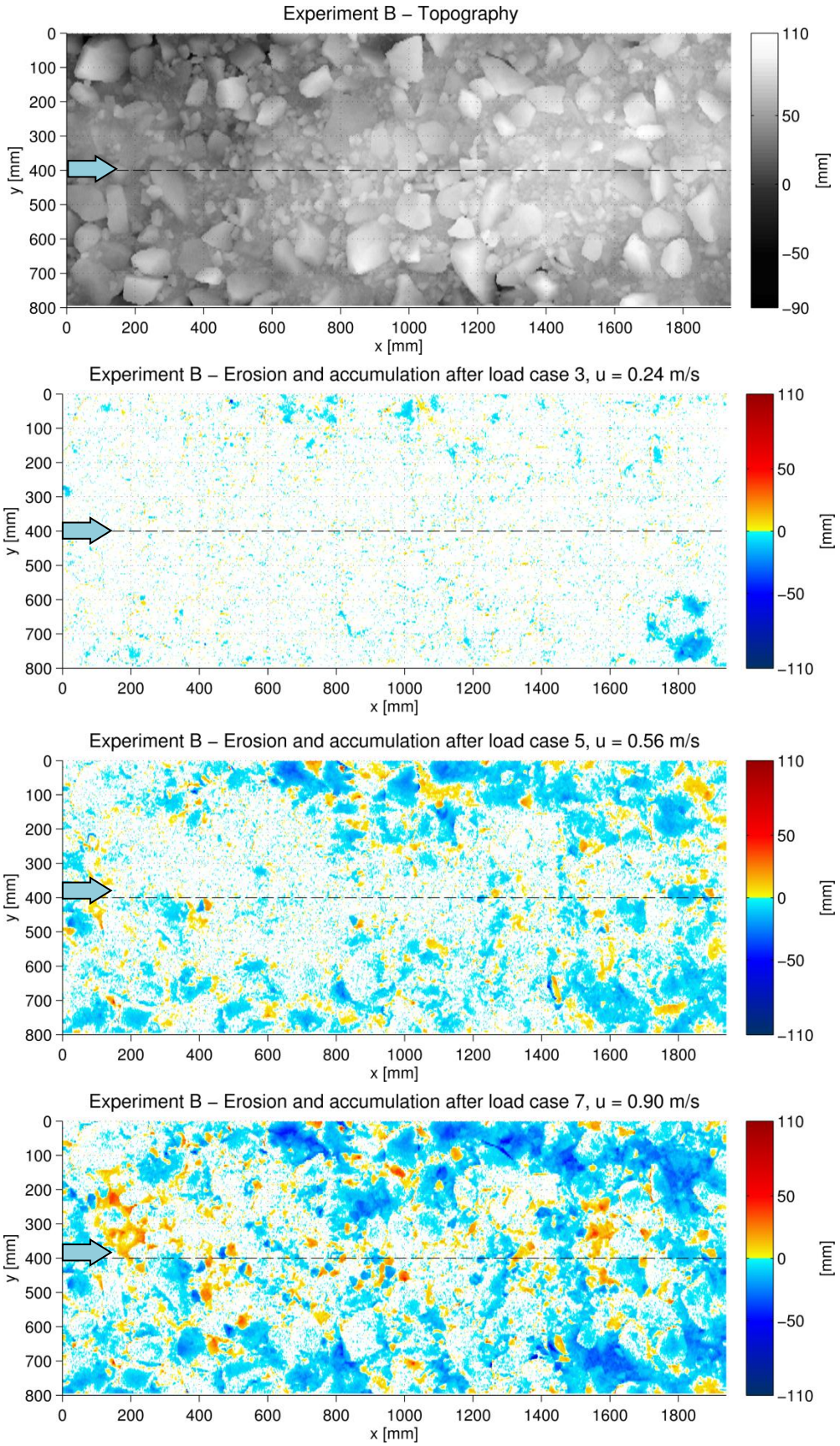

Figure 15: Development of erosion and accumulation areas at different flow velocities for experiment B. First figure shows the DEM of the bed surface at the beginning of experiment B based on laser scanning data.

Fractional critical shear stress

Fig. 16 shows the fractional critical shear stresses $\tau_{c,i}$ calculated with the Largest Grain Method for all three sediment samples and experiments, respectively. For all sediment samples the strong variation of critical shear stresses with the considered grain sizes d_i is apparent. Similar variations of $\tau_{c,i}$ are also pointed out by Kuhnle (1993) and Wilcock and Crowe (2003) for specific sediment mixtures and presented in Fig. 16 for comparison. Kuhnle (1993) investigated the incipient motion of sand-gravel sediment mixtures, which contained a gravel mix (d_{50} = 5.579 mm) and a sand mix (d_{50} = 0.476 mm). He found that in case of 100% sand or 100% gravel mixtures (Kuhnle (1993) Gravel), all grain sizes were eroded at the nearly the same critical bed shear stress. However, in the experiments with sand-gravel mixtures (Kuhnle (1993) SG45 with 45% gravel), the sand fractions were still moved at almost the same shear stress, whereas the critical shear stresses for the gravel fractions were significantly depending on the grain size. Wilcock and Crowe (2003) presented critical shear stresses for additional sand-gravel mixtures. They demonstrated, that the variation of the critical shear stress $\tau_{c,i}$ with grain sizes d_i increases with the amount of sand within the mixture and thus with the non-uniformity of the sediment mixture. In accordance with those findings, the critical shear stresses for the extremely wide-graded materials used in this paper vary strongly with grain size and therefore indicate a highly selective mobility of individual fractions for the investigated materials mixtures.

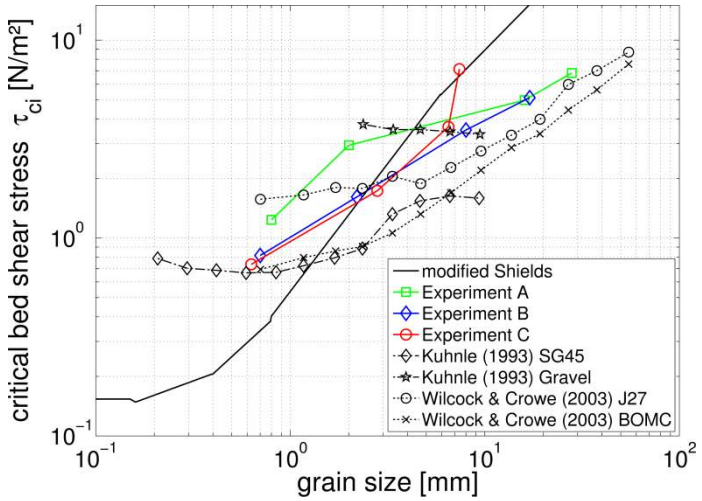

Figure 16: Critical shear stresses $\tau_{c,i}$ for corresponding grain sizes d_i.

Furthermore, Kuhnle (1993) and Wilcock and Crowe (2003) showed that the critical shear stresses $\tau_{c,50}$ for the d_{50} grain diameter of their sediment mixtures were quite close to the corresponding Shields values. In this present study the $\tau_{c,50}$ values could not be determined, because no grain sizes in the range of the d_{50} diameter of the sediment samples (25-72 mm) were collected by the sediment trap. This already indicates to much lower values of $\tau_{c,50}$ for the mixtures in this study compared to the Shields approach.

Discussion

Based only on the visual observations a high erosion stability of the material under current load could be conjectured. This contradicts the calculated critical shear stresses, which indicate a relative low erosion stability of coarser fraction with respect to the Shields approach. Available hiding functions, which consider exposition effects of coarser grains within the sediment mixtures, point to smaller critical shear stresses for these fractions. But usually it is assumed that fractions are affected by the exposition phenomenon, which are larger than the representative d_{50} mean diameter of the mixtures. In this study already much smaller fractions than the d_{50} diameter of the three sediment mixtures show smaller critical shear stresses as would have been expected by the Shields approach.

As pointed out by several authors and shown in summery by Shvidchenko et al. (2001), the Shields curve is not an appropriate mean to accurately assess the incipient motion of non-uniform sediment mixtures. However, the dimension of the differences by which the behavior of the tested sediment mixtures deviates from the prediction of the Shields curve, is unexpected.

Conclusions

In order to assess the stability and the performance of coarse grain materials as scour protection large-scale hydraulic model tests were carried out by the Franzius-Institute. The experimental study provided first insights in the behavior of coarse grain materials under wave and current load. The results indicate to an apparent high stability against spectral wave load and stationary current for the investigated wide-graded grain material and the given test conditions. In summary, the following results on the stability and scour performance of wide-graded grain materials under spectral wave load can be concluded from the first test phase:

- Along with general small changes of the bed topography under wave load, tendencies of a stabilizing amour layer development were observed.
- Development of a radial structure-induced scour pattern around the monopile, with two positions of almost identical maximum scour depth diagonal in front and on the back side of the monopile.
- A maximum structure-induced scour depth of S/D = 0.161 was observed after 9000 waves and a simulated storm duration of 20 h with a maximum significant wave height of H_s = 1.3 m. However, it has to be noted that this scour depth does not represent a final equilibrium scour depth.
- The final eroded scour volume amounts to 0.05 m³/m² within a radial distance from the center of the monopile of r/D = 1.5, which corresponds to a mean scour depth of 5 cm around the monopile. The calculation of the scour volume might be influenced by an asymmetrical scour pattern around the monopile in wave direction.

In addition, following conclusions regarding the erosion stability of wide-graded quarry-stone materials under stationary current can be drawn from the second test phase:

- Stable and immobile bed surfaces established, indicating the development of a temporarily static armor layer under stationary current. Therefore the development of a stabilizing armor layer may be considered in the design of scour and bed protection systems containing wide-graded quarry-stone material.
- The investigated wide-graded material showed a strong variation of critical shear stresses in dependency of grain size which indicates to a highly selective mobility of individual fractions. The Shields approach, which is still the method of choice for the stability assessment of granular scour and bed protections, is not able to represent the selective mobility of the applied wide-graded material. The Shields approach significantly overpredicts the critical shear stresses for the mean diameter d_{50} of the tested wide-graded material, despite the apparent erosion stability under stationary observed in this study

The applied wide-graded material appears promising regarding the application as scour or bed protection for estuarine and coastal structure, also due to the ability to develop a stabilizing armor layer under wave as well as under flow conditions and the associated increase in erosion stability. However, future studies have to focus on the further investigation of the involved erosion processes in order to fully understand the stabilizing process of wide-graded materials. Therefore, detailed measurements of the flow field above rough beds have to be performed and methods to measure or estimated bed shear stresses have to be refined.

Acknowledgements

The authors are thankful to the Mibau Holding GmbH for supporting this research. Furthermore, the authors wish to thank M. Bartels, M. Paehr and T. Freitag for their support in conducting the extensive hydraulic experiments.

REFERENCES

Andrews, E. D. (1983). Entrainment of gravel from naturally sorted riverbed material. Geological Society of America Bulletin, Vol. 94, 1225-1231.

Biron, P. M. et al. (2004). Comparing different methods of bed shear stress estimates in simple and complex flow fields. Earth Surf. Process. Landforms, Vol. 29, 1403-1415.

Carling, P. A. (1983). Threshold of coarse sediment transport in broad and narrow natural streams. Earth Surf. Process. Landforms, Vol. 8, 1-18.

CERC, Coastal Engineering Research Center. (2006). Coastal Engineering Manual.

De Vos, L., et al. (2011). Empirical design of scour protections around monopile foundations. Part 1: Static approach. Coastal Engineering, 58, 540-553.

Det Norske Veritas, DNV. (2010). DNV-OS-J101 Design of Offshore Wind Turbine Structures.

Germanischer Lloyd, GL. (2005). Rules and Guidelines, IV Industrial Services, 2 Guideline for the Certification of Offshore Wind Turbines. Hamburg : Germanischer LLoyd, 2005.

Jain, S. C. (1990). Armor or Pavement. Journal of Hydraulic Engineering, Vol. 116, 436-440.

Kuhnle, R. A. (1993). Incipient motion of sand-gravel sediment mixtures. Journal of Hydraulic Engineering, 119.

Marion, A. and Fraccarollo, L. (1997). Experimental investigation of mobile armoring development. Water Resources Research, Vol 33, 1447-1453.

Melville, B und Coleman, S. (2000). Bridge Scour. Water Resources Publications, 2000.

Parker, G. and Sutherland, A. J. (1990). Fluvial armor. Journal of Hydraulic Research, Vol 28, 529-544.

Petrie, J. et al. (2010). Local boundary shear stress estimates from velocity profiles measured with an ADCP. River Flow 2010, 1749-1755.

Shields, A. (1936). Anwendung der Ähnlichkeitsmechanik und der Turbulenzforschung auf die Geschiebebewegung. Berlin : Eigenverlag der Preußischen Versuchsanstalt für Wasserbau und Schiffbau, 1936.

Shvidchenko, A. B. et al. (2001). Critical shear stress for incipient motion of sand/gravel streambeds. Water Resources Research, Vol. 37, 2273-2283.

Soulsby, R. (1997). Dynamics of marine sands - A manual for practical applications. Thomas Telford, 1997.

Sumer, B. M., Fredsøe, J., Christiansen, N. (1992). Scour around vertical piles in waves. Journal of Waterway, Port, Coastal and Ocean Engineering., 118, 15-31.

Sumer, B. M., Fredsøe, J. (2001). Wave scour around a large vertical circular cylinder. Journal of Waterway, Port, Coastal and Ocean Engineering, 127, 125-134.

Sumer, B. M., Fredsøe, J. (2002). The mechanics of scour in the marine enviroment. Advanced Series on Ocean Engineering . 2002, Volume 17.

Whitehouse, R. (1998). Scour at marine structures: a manual for practical application. HR Wallingford.

Wilcock, P. R. (1988). Methods for Estimating the Critical Shear Stress of Individual Fractions in Mixed-Size Sediment. Water Resources Research, Vol. 24, 1127-1135.

Wilcock, P. R. and Crowe, J. C. (2003). Surface-based Transport Model for Mixed-Size Sediment. Journal of Hydraulic Engineering, Vol. 129, 120-128.

Zanke, Ulrich C.E., et al. (2011). Equilibrium scour depth around piles in noncohesive sediments under currents and waves. Coastal Engineering, 58.